Journal of Sound and Vibration 329 (2010) 2395–2409

Contents lists available at ScienceDirect

Journal of Sound and Vibration

journal homepage: www.elsevier.com/locate/jsvi

An experimental investigation of change detection in uncertain chain-like systems

Miguel R. Hernandez-Garcia [a], Sami F. Masri [a,*], Roger Ghanem [a], Eloi Figueiredo [b], Charles R. Farrar [c]

[a] Viterbi School of Engineering, University of Southern California, Los Angeles, CA 90089, USA
[b] Department of Civil Engineering, University of Porto, 4200-465 Porto, Portugal
[c] The Engineering Institute, Los Alamos National Laboratory, Los Alamos, NM 87545, USA

ARTICLE INFO

Article history:
Accepted 18 December 2009
The peer review of this article was organized by the Guest Editor
Available online 25 January 2010

ABSTRACT

Promising ongoing research on "smart" sensing technologies is offering low-cost alternatives and new opportunities for large-scale SHM. Networks of sensors with wireless communication and computational capabilities can be used to increase the spatial resolution of data collection while providing a distributed computing framework for implementing structural health monitoring algorithms. Robust and practical SHM methodologies being able to rapidly and accurately detect and assess changes in the monitored system are required to be at the core of these "smart" structures. A data-driven non-parametric identification technique is used to implement a robust change detection methodology for uncertain MDOF chain-like systems that can be implemented in densely distributed smart-sensor networks. Experimental data from a test-bed structure tested at Los Alamos National Laboratory are used to evaluate the effectiveness and reliability of the proposed SHM methodology. The results of this study showed that the proposed approach was able, in a rigorous statistical framework, to confidently detect the presence of structural changes, accurately locate the structural section where the change occurred, and provide an accurate estimate of the actual level of "change". Additionally, a full-order finite element model of the test structure, as well as the results from the experimental modal identification using the ERA algorithm were employed to validate the results obtained in this change-detection study.

1. Introduction

1.1. Background and motivation

During last years, the potential benefits that structural health monitoring (SHM) can have in the performance, serviceability, and reliability of aerospace, civil and mechanical structures have been recognized and demonstrated worldwide through the extensive technical literature available in this emerging field. Several illustrative applications can be found in the proceedings of the International and European Workshops on Structural Health Monitoring [1,2], the World Conference on Structural Control and Monitoring [3,4], and the SPIE Conferences on Smart Structures and Materials & Non-destructive Evaluation and Health Monitoring [5,6].

* Corresponding author. Tel.: +1 213 7400602.
E-mail addresses: miguelrh@usc.edu (M.R. Hernandez-Garcia), masri@usc.edu (S.F. Masri), ghanem@usc.edu (R. Ghanem), eloi.figueiredo@fe.up.pt (E. Figueiredo), farrar@lanl.gov (C.R. Farrar).

0022-460X/$ - see front matter © 2009 Elsevier Ltd. All rights reserved.
doi:10.1016/j.jsv.2009.12.024

Extensive research on the core technical areas of structural health monitoring—modeling, measurements, data analysis and prediction [7]—have led to a significant number of well-developed vibration-based damage identification algorithms and sensing technologies. Despite all these advancements, realizing field-deployable and continuous online SHM with centralized data acquisition, processing, and analysis has been challenging. Densely distributed sensor networks, which are required to monitor the condition of individual components and/or the entire system in most of the real large-scale applications, are still restricted by current limitations in the hardware (i.e., wired or wireless sensors) and software (i.e., damage identification methods). The use of dense array of sensors, especially at high sampling frequencies, is needed in order to capture the effects that structural changes have in the systems' dynamic response.

Promising ongoing research on "smart" embedded sensing technologies is offering low-cost alternatives and new opportunities for large-scale SHM. Sensors with on-board microprocessors powered by energy harvesting or microbatteries and featuring computational, sensor diagnostic, and reconfigurable wireless communication (i.e., multihop protocols) capabilities, can be used to increase the spatial resolution of data collection while providing a distributed computing framework for implementing structural health monitoring algorithms. Robust and practical SHM methodologies being able to rapidly and accurately detect and assess changes in the monitored system are required to be at the core of these "smart" sensors. Although some approaches have been validated in the laboratory [8–10], there are some unavoidable factors in real structures that SHM strategies, exploiting the "smart" sensors capabilities, have to still cope with: the presence of intrinsic and damage-associated nonlinearities (e.g., hysteresis, gaps, sliding friction); the inherent stochastic nature of the systems' components (i.e., randomness in the structural properties and materials); the variability in environmental or operational conditions; and the uncertainties in the modeling, measurement and data analysis processes.

Excellent and careful reviews of existing methods and technologies, as well as recent publications summarizing the state-of-the-art of SHM can be found in Doebling et al. [11], Peeters and De Roeck [12], Sohn et al. [13], Van der Auweraer and Peeters [14], Staszewski et al. [15], Inman et al. [16], Kerschen et al. [17], Park and Sohn [18], Adams [7], Brownjohn [19], Farrar et al. [20], Farrar and Worden [21], Friswell [22], Glaser et al. [23], Lynch [24], Nagayama and Spencer [9], Park and Inman [25] and Sohn [26].

Over the years, several approaches for constructing computationally efficient, model-free representations of single-degree-of-freedom (SDOF) and multi-degree-of-freedom (MDOF) systems have been successfully applied to synthetic and experimental data [27–31]. Among these approaches, a time-domain non-parametric identification technique for chain-like MDOF systems presented by Masri et al. [27] is of special interest. The decomposition strategy of this technique makes it suitable to exploit the distributed computing capabilities of smart sensors.

1.2. Scope

In this exploratory study, the decomposition approach presented in the above-mentioned reference is used to implement a robust data-driven change detection methodology for uncertain chain-like systems that can be implemented in densely distributed smart-sensor networks. The chain-like system topology encompasses many practical applications including tall buildings, transmission towers, offshore platforms, wind turbines and airplane wings. Experimental data from a test-bed structure tested at Los Alamos National Laboratory are employed to validate the proposed approach. A stochastic description of the detected changes is additionally used to assess the methodology's range of detectability and reliability. An overview of the chain-like system identification approach is provided in Section 2; the description of the test-bed structure, implementation details of the change detection methodology, and the statistical analysis and discussion of the results are all presented in Section 3.

2. Chain-like system identification approach

Consider an MDOF chain-like system, consisting of a series of lumped masses m_i interconnected by n arbitrary unknown (non-necessarily) nonlinear elements $G^{(i)}$, subjected to a base motion x_0, and/or directly applied forces F_i. The elements' restoring forces are assumed to depend on the relative displacement and velocity across the terminals of each element, in addition to a set of specific parameters $\boldsymbol{p}$ that characterize the various types of nonlinearities. The differential equations of motion for the system under discussion, shown in Fig. 1(a), can be written as [27,32]

$$G^{(n)}(z_n,\dot{z}_n,\boldsymbol{p})=\frac{F_n}{m_n}-\ddot{x}_n$$

$$G^{(i)}(z_i,\dot{z}_i,\boldsymbol{p})=\frac{F_i}{m_i}-\frac{m_{i+1}}{m_i}\ddot{x}_i+G^{(i+1)}(z_{i+1},\dot{z}_{i+1},\boldsymbol{p}) \qquad \text{for } i=n-1,n-2,\ldots,1 \tag{1}$$

where $G^{(i)}(z_i,\dot{z}_i,\boldsymbol{p})$ is the mass-normalized restoring force function of the element $G^{(i)}$, $\ddot{x}_i$ is the absolute acceleration of the mass m_i, with z_i and $\dot{z}_i$ being the relative displacements and velocities between two consecutive masses. These relative motion variables can be obtained from the absolute state variables of the masses and the moving support.

From Eq. (1), it is clearly seen that the restoring forces acting on all elements in the chain-like system can be sequentially determined by starting the data processing from the n th (tip) element of the chain. Within the context of this

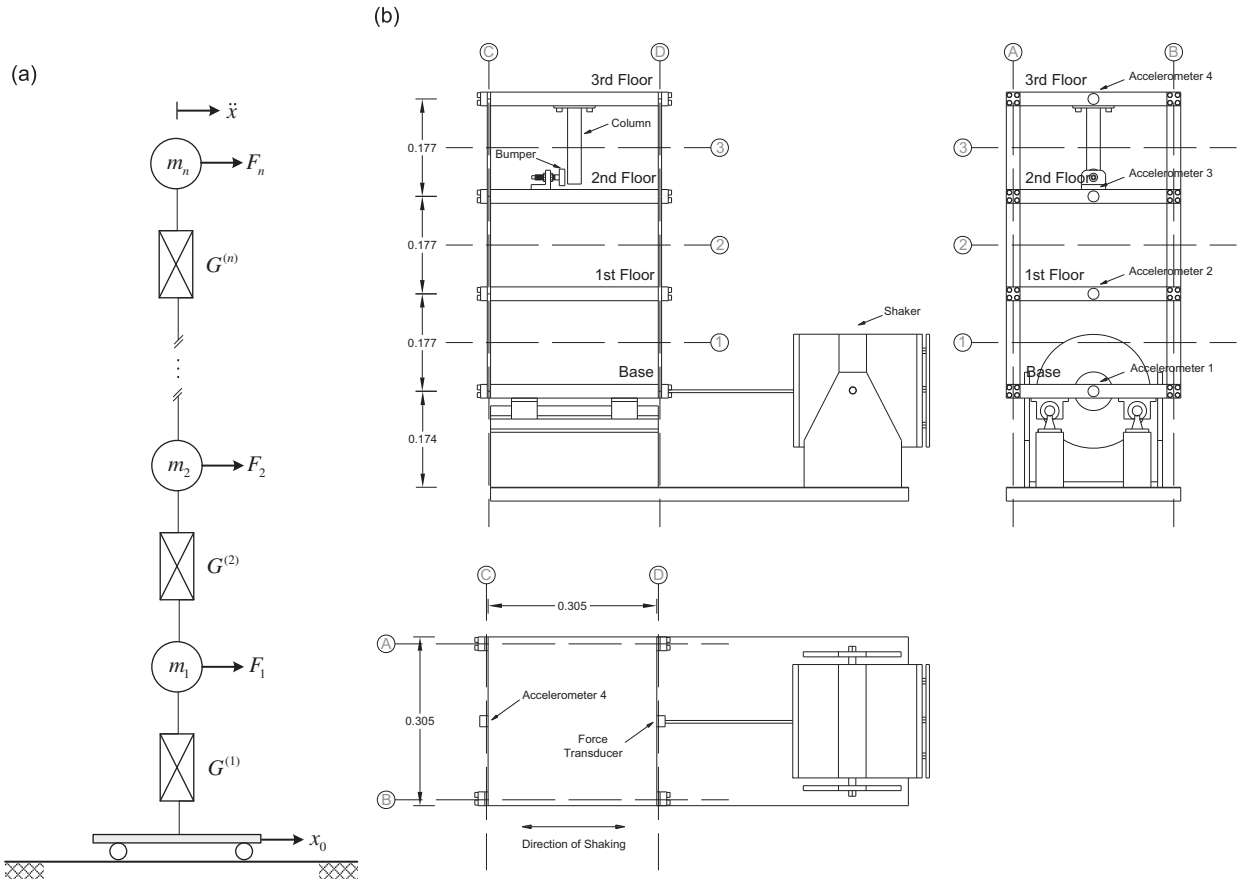

Fig. 1. (a) Typical structural topology for a nonlinear MDOF chain-like system. (b) LANL-4DOF test-bed structure schematic drawings.

method, the absolute accelerations $\ddot{x}_i$ are assumed to be available from measurements, as well as the applied forces F_i, the base excitation x_0 and the magnitude of the lumped masses m_i.

After obtaining all the restoring force time histories, it is possible to generate a non-parametric representation for each element, in terms of a truncated doubly indexed series expansion in a suitable basis, that approximates the real restoring force function [33,28,29,34]. The approximating representation $\hat{G}^{(i)}(z_i, \dot{z}_i)$ for the obtained restoring forces, in an orthogonal polynomial basis, is given by the following expression:

$$G^{(i)}(z_i, \dot{z}_i, \boldsymbol{p}) \approx \hat{G}^{(i)}(z_i, \dot{z}_i) = \sum_{q=0}^{q_{max}} \sum_{r=0}^{r_{max}} C_{qr}^{(i)} T_q(z_i') T_r(\dot{z}_i') \tag{2}$$

where $C_{qr}^{(i)}$ are the Chebyshev series coefficients, $T_k(\cdot)$ is the Chebyshev polynomial of order k, and z_i', $\dot{z}_i'$ are the normalized relative state variables. Subsequently, each of the estimated restoring forces can be expressed as a power series of the form

$$\hat{G}^{(i)}(z_i, \dot{z}_i) = \sum_{q=0}^{q_{max}} \sum_{r=0}^{r_{max}} a_{qr}^{(i)} z_i^q \dot{z}_i^r \tag{3}$$

where $a_{qr}^{(i)}$ are constant coefficients, and z_i, $\dot{z}_i$ are the relative state variables.

The application of this non-parametric identification approach allows the capture of the dominant features of the nonlinear elements into reduced-order, model-free representations [29]. Due to the fact that the non-parametric representation of the restoring force depends on the relative state variables, the numerical implementation of the chain-like system identification approach requires the availability of displacement and velocity time-histories, which can be obtained by digital signal processing of the measured accelerations. The advantage of this formulation is that the identification of a MDOF system can be decomposed into a process where each of the elements in the system is identified independently. Furthermore, since the identification of each element is done individually, this procedure can be easily implemented in a distributed computing framework. It should be emphasized that since this approach is entirely data-driven, the number of degrees-of-freedom in the considered chain-like system will be determined by the number of available sensors deployed on the structure.

3. Change detection in a MDOF test-bed structure

Experimental data from a test-bed structure, that has been tested at the Los Alamos National Laboratory (LANL), were used to illustrate the application of the methodology under discussion in detecting structural changes in the system. Full details concerning this LANL test setup are documented in [35].

3.1. LANL test-bed structure

The laboratory three-storey shear-building structure (see Fig. 1) consists of four aluminum plates ($30.5 \times 30.5 \times 2.5$ cm) connected by bolted joints to four aluminum columns ($17.7 \times 2.5 \times 0.6$ cm) at each floor. An additional element ($15 \times 2.5 \times 2.5$ cm) attached to the top floor and an adjustable bumper mounted on the second floor can be used to introduce a gap nonlinearity in the system. The gap distance can be modified by adjusting the position of the bumper to vary the level of the nonlinearity. The whole structure is mounted on two rails to allow the system to slide only in one direction. An electro-dynamic shaker was used to provide a band-limited random base excitation (20−150 Hz) to the test structure.

The deployed sensor network consists of four accelerometers and a force transducer with nominal sensitivities of 1000 mV/g and 2.2 mV/N, respectively. The accelerometers were attached to each aluminum plate, along a vertical center line, to measure the dynamic response of the 4DOF lab structure. The force transducer was connected to the tip of the stinger to gauge the input force generated by the shaker. The sensor's measurements were recorded at a sampling frequency of 322.58 Hz by a data acquisition system.

The structural changes in the system were physically simulated through pure variations in either the mass or stiffness of the reference structure. The mass of the system was modified by attaching a 1.2 kg concentrated mass to the aluminum plates, while the changes in stiffness were introduced by reducing by half the cross-section thickness of selected columns. This change in the cross-section corresponded to a 87.5% reduction in the column's stiffness. The nine structural state configurations considered in this study are summarized in Table 1. A total of 90 acceleration data sets, involving all structural configurations, were obtained from ten experimental tests performed under different external force realizations (i.e., 10 data sets for each system configurations) in order to account for the variability in the data. Although the test-bed structure had an adjustable nonlinear gap in the third storey, it was set to keep the system within the linear range during the dynamic tests considered in this study.

3.2. Sample data processing results

For the purposes of this study, the test-bed structure was considered as a 3DOF chain-like system subjected to base motions, hence the simplified equations of motion (Eq. 1) could be rewritten as:

$$G^{(3)}(z_3, \dot{z}_3, \boldsymbol{p}) = -\ddot{x}_3$$

$$G^{(2)}(z_2, \dot{z}_2, \boldsymbol{p}) = -\frac{m_3}{m_2}\ddot{x}_2 + G^{(3)}(z_3, \dot{z}_3, \boldsymbol{p})$$

$$G^{(1)}(z_1, \dot{z}_1, \boldsymbol{p}) = -\frac{m_2}{m_1}\ddot{x}_1 + G^{(2)}(z_2, \dot{z}_2, \boldsymbol{p}) \tag{4}$$

In addition, only the acceleration time-histories recorded by the four accelerometers and the floor mass *ratios* $\overline{m}_i = m_{i+1}/m_i$ were assumed to be available. Because the system's mass is approximately uniformly distributed throughout the structure, the mass *ratios* $\overline{m}_i$ were considered equal to one. Since the displacement and velocity time-histories at measurement stations are required to apply this identification approach, the acceleration records were windowed, detrended, band-pass filtered and integrated. Typical top floor vibration records, including the measured accelerations and corresponding computed velocities and displacements, are shown in Fig. 2(a). Note that the system displacements are on the order of one tenth of a millimeter.

Table 1
Summary of structural state conditions.

State	Condition	Description
State#1	Reference condition	–
State#2	19.1% base mass increment	1.2 kg additional mass on the base
State#3	19.1% 1st-storey mass increment	1.2 kg additional mass on the 1st storey
State#4	21.8% 1st-storey stiffness reduction	87.5% stiffness reduction in column 1BD 1st storey)
State#5	43.7% 1st-storey stiffness reduction	87.5% stiffness reduction in columns 1AD and 1BD (1st storey)
State#6	21.8% 2nd-storey stiffness reduction	87.5% stiffness reduction in column 2BD (2nd storey)
State#7	43.7% 2nd-storey stiffness reduction	87.5% stiffness reduction in columns 2AD and 2BD (2nd storey)
State#8	21.8% 3rd-storey stiffness reduction	87.5% stiffness reduction in column 3BD (3rd storey)
State#9	43.7% 3rd-storey stiffness reduction	87.5% stiffness reduction in columns 3AD and 3BD (3rd storey)

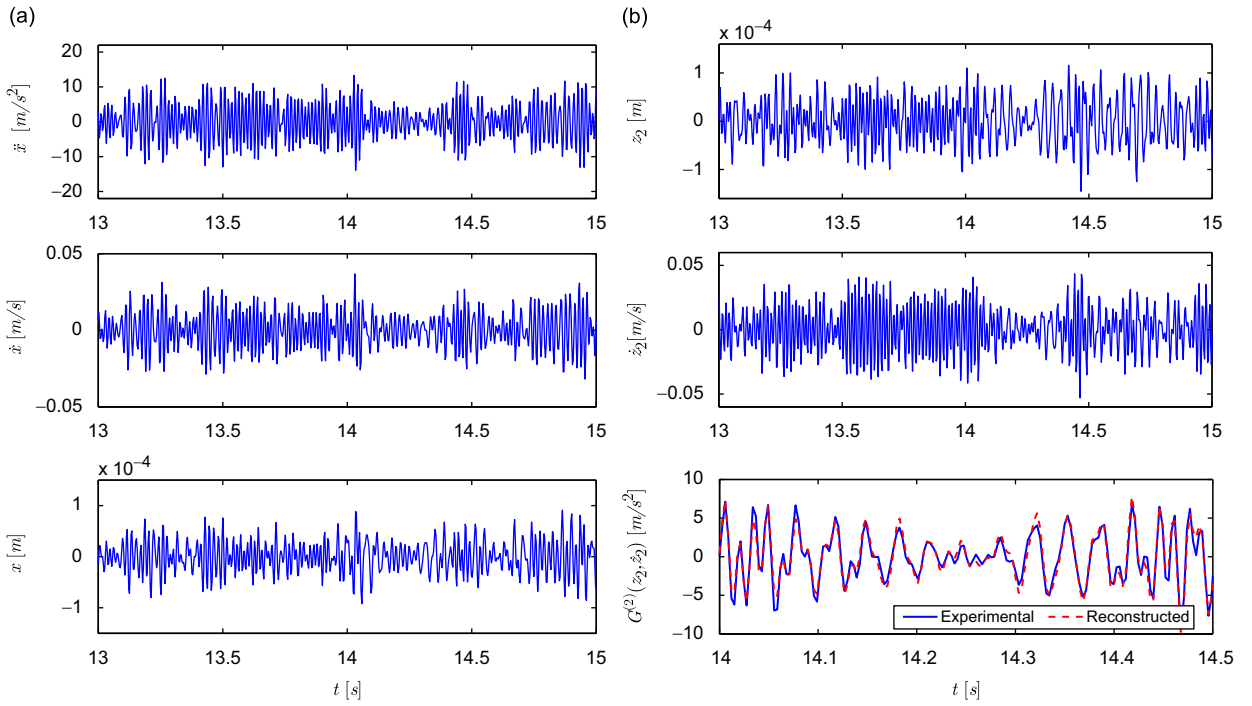

Fig. 2. (a) Typical acceleration, velocity and displacement records obtained at 2nd floor. (b) Relative displacement and velocity time-histories computed between masses m_2 and m_1 are shown in the first two rows of this figure. The third row corresponds to a comparison between the measured restoring force time-history for element $G^{(2)}$ and the reconstructed time-history using the identified restoring force coefficients (virtually identical curves).

Due to the limited experimental data available, all vibration records were divided into overlapped segments of 6.34 seconds, which include more than 100 fundamental periods of the system, so as to obtain an enlarged collection of acceleration, velocity and displacement time-histories. In total, 150 ensembles of time-history records were generated for each of the structural configurations.

Once the relative displacements and velocities had been computed, the proposed time-domain identification technique is then applied to the ensembles of vibration record segments to build the associated non-parametric reduced-order models for each element in the 3DOF chain-like system, by determining the corresponding restoring force coefficients. The first two plots in Fig. 2(b) illustrate sample time-histories of relative displacements and velocities computed between the second and first floor of the 3DOF system in its reference structural configuration. The third plot depicts the time-history records of the measured and reconstructed mass-normalized restoring forces (basically identical curves) in solid and dashed lines, respectively, for the element $G^{(2)}$ connecting the first and second stories. Fig. 3(a) shows, as it is expected for linear elements, the estimated planar restoring force surfaces over the normalized phase space for the reference condition (i.e., state#1). The reconstructed mass-normalized restoring forces $\hat{G}^{(i)}(z_i,\dot{z}_i)$ were computed using the estimated coefficients and the corresponding sequence of Chebyshev polynomials in the relative state variables.

It should be noted that, although the structure was kept within the linear range during the dynamic tests, for the identification purposes of this study, the system was *not* assumed linear. The restoring force identification was initially carried out using Chebyshev polynomials of third-order in both normalized variables z' and $\dot{z}'$. A relative-contribution analysis of the identified $C_{qr}^{(i)}$ indicated that the linear terms had the most significant contributions to the restoring forces while the effect of the nonlinear terms were negligible. The non-parametric models for the elements $G^{(i)}$, in the reference and modified structural configurations, were then reduced to their corresponding first-order expansions by using the orthogonality property of the identified Chebyshev coefficients [33].

3.3. Change detection

As a consequence of structural changes, the dynamic characteristics and response time-histories of any chain-like system are affected; hence, the estimated restoring force surface of the interconnecting elements will exhibit variations with respect to the reference case. In Fig. 3(b), the changes in the identified restoring force surface for the elements $G^{(3)}$, $G^{(2)}$ and $G^{(1)}$ caused by 43.75% second-storey stiffness reduction (i.e., state#7) are displayed. From Eqs. (2) and (3), it is observed that for a given order in the double-indexed expansion, variations in the restoring force would have effects on the identified coefficients, since they characterize the governing dynamic features of the system. This makes the restoring force coefficients a suitable set of parameters for change detection applications [29,30,34].

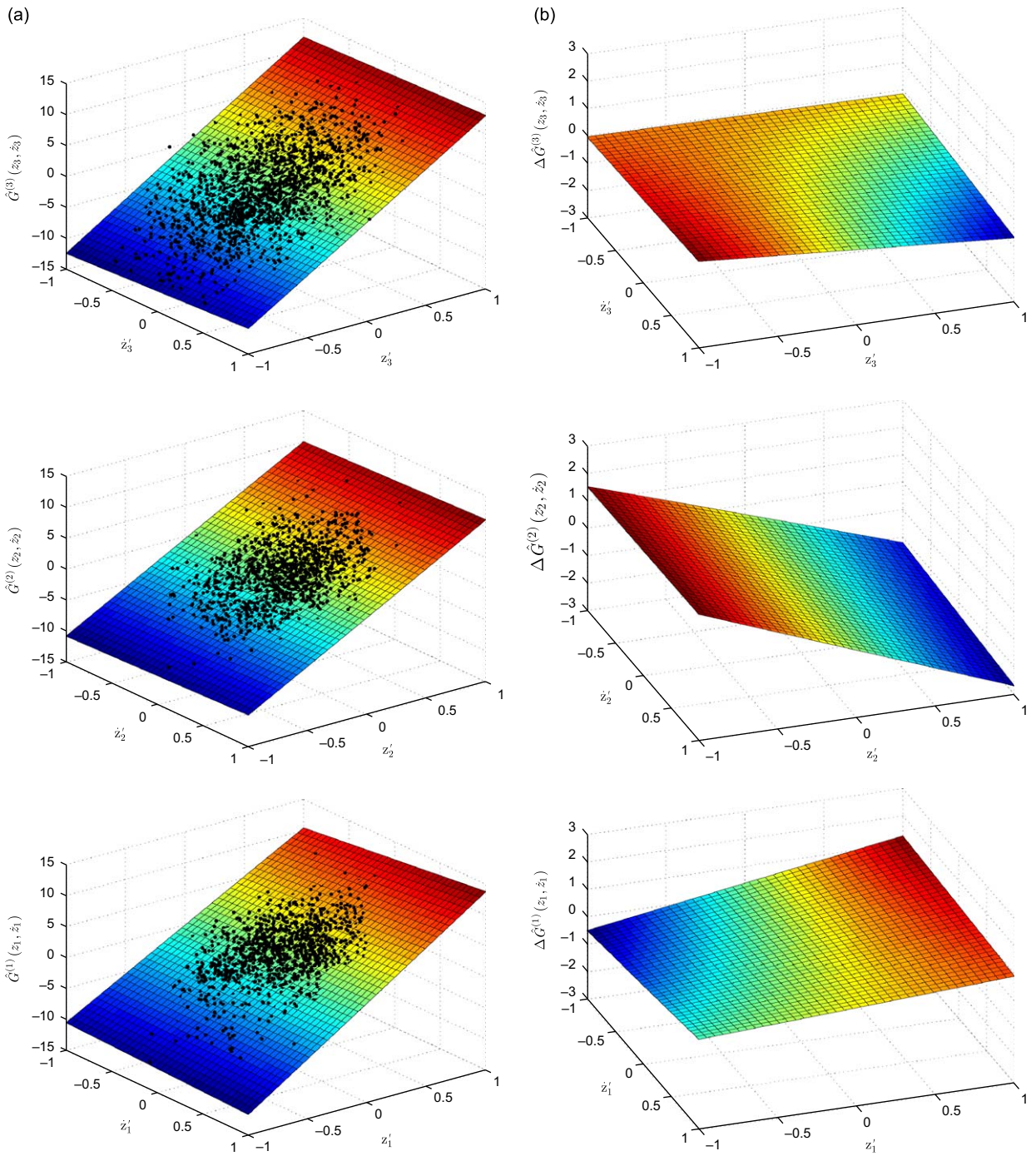

Fig. 3. (a) Identified restoring force surface for elements $G^{(3)}$, $G^{(2)}$ and $G^{(1)}$ in the reference structural condition. (b) Identified change in the restoring force surfaces in $G^{(3)}$, $G^{(2)}$ and $G^{(1)}$ due to a 43.75% second-storey stiffness reduction. Note that, for enhanced viewing, different amplitude scales are used in the LHS and RHS columns of plots.

Despite the fact that the Chebyshev coefficients $C_{qr}^{(i)}$ have several useful properties (i.e., orthogonality and unbiasness with respect to model complexity) for the identification and detection of changes in linear and nonlinear systems [34], their use in a stochastic framework is inconvenient since they rely on normalized variables [36]. Consequently, the equivalent de-normalized restoring force coefficients $a_{qr}^{(i)}$, corresponding to the dominant terms in the expansion, were selected instead as the features to be used and analyzed in this experimental study of change detection in uncertain chain-like systems.

Since the mass-normalized restoring force function for linear elements can be expressed as:

$$G^{(i)}(z_i,\dot{z}_i)=\frac{k_i}{m_i}z_i+\frac{c_i}{m_i}\dot{z}_i=\overline{k}_i z_i+\overline{c}_i\dot{z}_i=a_{10}^{(i)}z_i+a_{01}^{(i)}\dot{z}_i \tag{5}$$

the changes in mass and stiffness introduced in the LANL test-bed structure can be detected and quantified through direct analysis of the $a_{10}^{(i)}$ and $a_{01}^{(i)}$ coefficients, which hereafter are going to be also called the "mass-normalized stiffness-like" and "mass-normalized damping-like" terms, respectively. The global modal parameters of the system can be determined through the eigen decomposition of the global $M^{-1}K$ and $M^{-1}C$ matrices, which are given by the following expressions:

$$M^{-1}K=\begin{bmatrix} a_{10}^{(1)}\overline{m}_0 & -a_{10}^{(1)}\overline{m}_0 & 0 & 0\\ -a_{10}^{(1)} & a_{10}^{(1)}+a_{10}^{(2)}\overline{m}_1 & -a_{10}^{(2)}\overline{m}_1 & 0\\ 0 & -a_{10}^{(2)} & a_{10}^{(2)}+a_{10}^{(3)}\overline{m}_2 & -a_{10}^{(3)}\overline{m}_2\\ 0 & 0 & -a_{10}^{(3)} & a_{10}^{(3)} \end{bmatrix} \tag{6}$$

$$M^{-1}C=\begin{bmatrix} a_{01}^{(1)}\overline{m}_0 & -a_{01}^{(1)}\overline{m}_0 & 0 & 0\\ -a_{01}^{(1)} & a_{01}^{(1)}+a_{01}^{(2)}\overline{m}_1 & -a_{01}^{(2)}\overline{m}_1 & 0\\ 0 & -a_{01}^{(2)} & a_{01}^{(2)}+a_{01}^{(3)}\overline{m}_2 & -a_{01}^{(3)}\overline{m}_2\\ 0 & 0 & -a_{01}^{(3)} & a_{01}^{(3)} \end{bmatrix} \tag{7}$$

Notice that these matrices were reconstructed by modeling the three-storey structure as a 4DOF shear building [35].

By virtue of the normalization procedure embedded in the Chebyshev coefficients, it can be shown that the relative changes in the Chebyshev and de-normalized power-series coefficients are related by the equations:

$$\frac{\Delta C_{10}}{C_{10}^r}=\frac{a_{10}(z_{max}-z_{min}-z_{max}^r+z_{min}^r)+\Delta a_{10}(z_{max}-z_{min})}{a_{10}(z_{max}^r-z_{min}^r)} \tag{8}$$

$$\frac{\Delta C_{01}}{C_{01}^r}=\frac{a_{01}(\dot{z}_{max}-\dot{z}_{min}-\dot{z}_{max}^r+\dot{z}_{min}^r)+\Delta a_{01}(\dot{z}_{max}-\dot{z}_{min})}{a_{01}(\dot{z}_{max}^r-\dot{z}_{min}^r)} \tag{9}$$

where $(\cdot)^r$ denotes the variables associated with the reference case. Clearly, straight interpretation of variations in Chebyshev coefficients as genuine changes in the structure can be misleading because of their dependence on the extreme values of the relative state variables.

It is worth pointing out that, although the identification results for all structural conditions considered in this study indicated that the interstorey restoring forces were entirely characterize by the $a_{10}^{(i)}$ coefficients, which is foreseen for shear building-type structures, the coefficients $a_{01}^{(i)}$ were also considered for the sake of completeness.

3.4. Implementation and statistical analysis

The results of implementing the chain-like system identification to build data-driven reduced-order models of the LANL test-bed structure, and using the associated restoring force coefficients to detect structural changes in the system, are reported in this section.

The second-order statistics of coefficients $a_{10}^{(i)}$ and $a_{01}^{(i)}$, obtained from all data ensembles and for each structural state condition, are summarized in Table 2. Looking at the mean μ and coefficient of variation δ of the restoring force coefficients, it is noted that the mass-normalized stiffness-like coefficients have a low variability, with coefficients of variation ranging from 2% to 6%, compared to the more scattered mass-normalized damping-like coefficients (i.e., coefficients of variation between 50% and 250%). The dispersion of each coefficient is evidently related to the level of importance (contribution) in the characterization of the restoring forces. Clearly, from the change detection point of view, the $a_{10}^{(i)}$ coefficients are much more robust than the $a_{01}^{(i)}$ coefficients. Since the structure was tested under controlled laboratory conditions, the statistical variability in the restoring force coefficients $a_{10}^{(i)}$ and $a_{01}^{(i)}$ observed in this experimental study is basically due to modeling, measurement, and data processing errors.

In order to have a more appropriate description and characterization of the randomness in the restoring force coefficients, their underlying probability distributions have to be estimated. In an initial exploratory data analysis, normal probability plots indicated that even though the mass-normalized coefficients within the first and third quartiles could be reasonable assumed to have normal distributions, they deviated from Gaussianity in the tails of the distributions. This non-Gaussianity in the distribution of the $a_{10}^{(i)}$ and $a_{01}^{(i)}$ coefficients can be attributable to inherent nonlinearities in the system's dynamic properties as well as the model-order reduction performed in the identification procedure [29]. In Fig. 4(a), the (representative example) probability plots of the second-floor coefficients identified from the reference condition are shown. Finally, the stochastic representations for the identified coefficients $a_{10}^{(i)}$ and $a_{01}^{(i)}$, for all structural conditions, were obtained by kernel density estimation. Fig. 4(b) displays the histograms of the mass-normalized stiffness-like and

Table 2
Summary of mean (μ) and coefficient of variation (δ) of the identified restoring force coefficients for the LANL test-bed structure.

State	1st floor				2nd floor				3rd floor			
	$a_{10}^{(1)}=\overline{k}_1$		$a_{01}^{(1)}=\overline{c}_1$		$a_{10}^{(2)}=\overline{k}_2$		$a_{01}^{(2)}=\overline{c}_2$		$a_{10}^{(3)}=\overline{k}_3$		$a_{01}^{(3)}=\overline{c}_3$	
	μ ($\times 10^4$)	δ	μ	δ	μ ($\times 10^4$)	δ	μ	δ	μ ($\times 10^4$)	δ	μ	δ
State#1	7.121	0.040	10.665	0.716	6.390	0.048	5.742	1.229	6.733	0.035	3.795	1.057
State#2	7.039	0.039	10.460	0.571	6.421	0.045	3.487	1.745	6.728	0.027	3.933	1.340
State#3	5.830	0.031	9.039	0.520	6.334	0.045	6.282	1.057	6.703	0.043	4.776	1.077
State#4	5.513	0.042	6.468	0.764	6.174	0.054	7.975	0.747	6.618	0.033	4.076	1.155
State#5	4.092	0.040	1.965	2.580	6.179	0.040	6.422	1.061	6.547	0.032	2.479	1.816
State#6	7.053	0.041	10.958	0.519	4.836	0.041	5.511	0.891	6.611	0.026	3.790	0.981
State#7	7.187	0.032	10.174	0.597	3.597	0.035	5.357	0.717	6.572	0.026	3.944	1.004
State#8	7.223	0.062	7.665	0.968	6.700	0.051	3.166	1.541	5.269	0.031	2.197	1.759
State#9	7.303	0.058	8.799	0.736	6.486	0.039	3.055	1.686	3.765	0.025	2.273	1.249

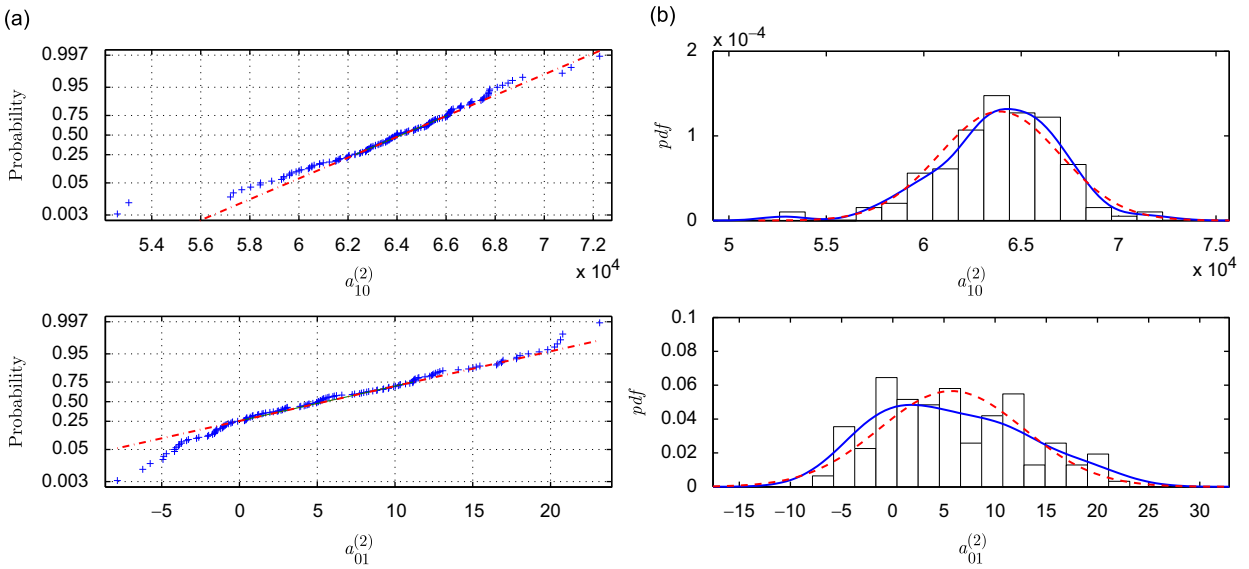

Fig. 4. Statistical representation of the identified restoring force coefficients for the reference structural condition. (a) Normal probability plots of the mass-normalized stiffness-like $a_{10}^{(2)}$ and mass-normalized damping-like $a_{01}^{(2)}$ coefficients. (b) Corresponding histograms, estimated probability density functions by kernel density estimators (solid lines) and superposed Gaussian distributions (dashed lines).

mass-normalized damping-like coefficients for the second-floor element in the baseline structural condition, the estimated probability density functions (solid lines), as well as the corresponding superposed Gaussian distributions (dashed lines).

To facilitate the visual analysis of the results for detecting structural changes in the LANL test structure, the probability density functions of the reference-normalized coefficients $\tilde{a}_{mn}^{(i)}=(a_{mn}^{(i)}-{}^{r}\overline{a}_{mn}^{(i)})/{}^{r}\overline{a}_{mn}^{(i)}$, where ${}^{r}\overline{a}_{mn}^{(i)}$ indicates the mean value of the coefficients $a_{mn}^{(i)}$ from the reference condition, were estimated for all the structural conditions listed in Table 1. Figs. 5–8 display the pdfs of $\tilde{a}_{10}^{(i)}$ and $\tilde{a}_{01}^{(i)}$ for the baseline condition in solid lines, while the probability functions from the modified structural configurations are plotted with dot-dashed and dashed lines. First (top) rows correspond to third-storey coefficients; middle rows to second-storey, and bottom rows to first-storey.

Two normalized indices $\Delta\mu/\mu_r$ and $\Delta\mu/\sigma_r$ were additionally employed to assess the effectiveness and robustness of the chain-like system identification approach in detecting and localizing structural changes. These dimensionless indices are found by dividing the difference in the mean values of the estimated restoring force coefficients ($\Delta\mu=\mu-\mu_r$) by the corresponding means (μ_r) and standard deviations (σ_r) from the reference case. The dimensionless index $\Delta\mu/\mu_r$, which corresponds to the relative change in the coefficients, can be used intuitively to assess the magnitude or level of "change" in the system, while a measure of the statistical significance of the detected changes can be gauged by the ratio $\Delta\mu/\sigma_r$, which is also known as the signal-to-noise ratio (SNR). Relatively large values of the latter index indicate that the existing mean differences are not attributable just to the normal variability within the coefficients and therefore, they can be associated with "genuine" changes in the system [30]. In this study, a rough threshold for detection of

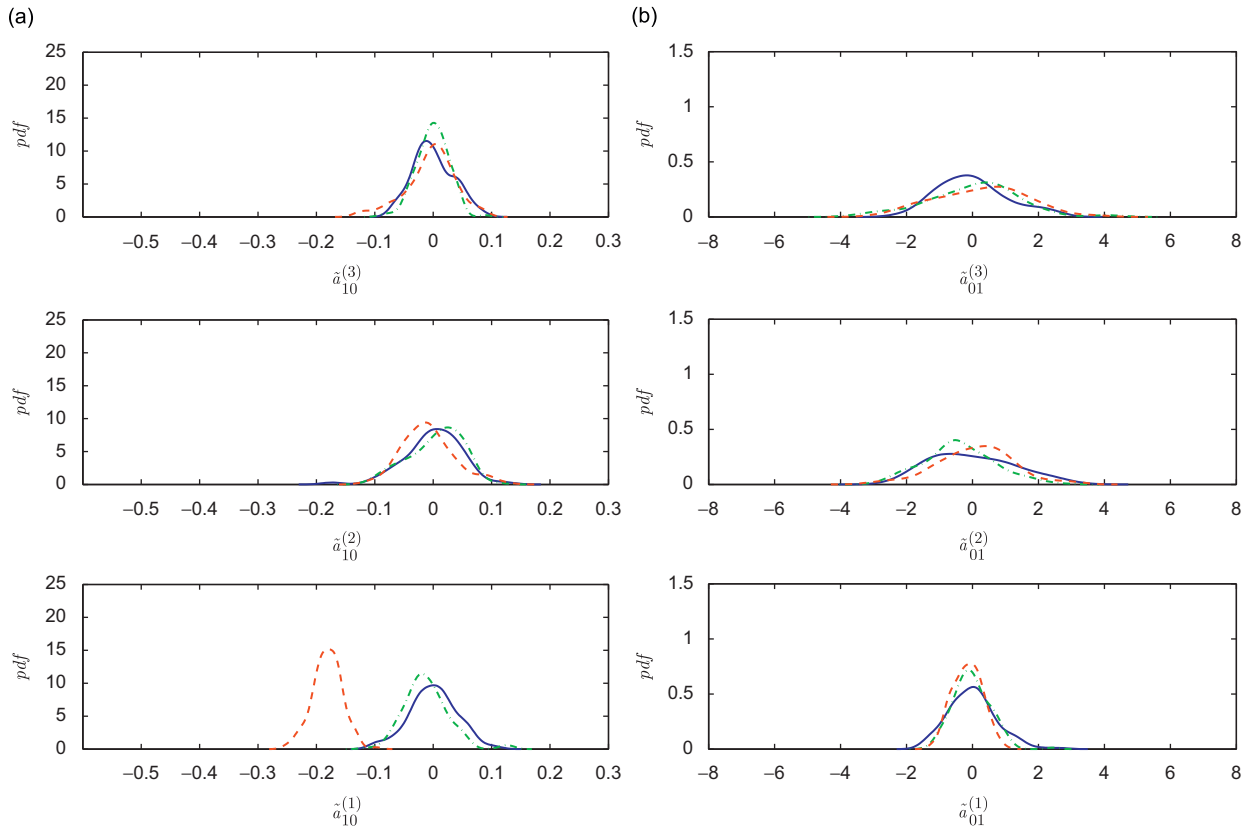

Fig. 5. Comparison of probability density functions of identified mass-normalized stiffness-like and mass-normalized damping-like coefficients. The solid lines correspond to the pdf of the coefficients in the baseline condition. The dot-dashed and dashed lines show the coefficients' pdf obtained in state#2 and state#3, respectively. (a) Normalized stiffness-like coefficients ($\tilde{a}_{10}^{(i)}$) and (b) Normalized damping-like coefficients ($\tilde{a}_{01}^{(i)}$).

$|\Delta\mu/\sigma_r| \geq 2.0$ was established to determine, with at least a 95% of confidence, when significant changes had occurred in the $a_{10}^{(i)}$ and $a_{01}^{(i)}$ coefficients. The values of $\Delta\mu/\mu_r$ and $\Delta\mu/\sigma_r$ for all eight scenarios with structural changes are summarized and presented in Table 3. Table entries in boldface correspond to actual structural changes that were detected correctly.

For the state#2 scenario, the tabulated results showed that the relative changes in the mean values of all the restoring force coefficients, including the 40% reduction in the damping-like coefficient for the second floor, were not significant since all $\Delta\mu/\sigma_r$ were below the previously defined threshold. Therefore, by counting on the experimental results, the presence of structural changes, in this case, is ruled out because the fluctuations on the mean values can be associated with the randomness of the estimated restoring force coefficients. Notice that, in this scenario, an additional mass was placed at the baseplate of the structure. It is important to highlight that detecting structural changes located at the system's base level, are beyond the capabilities of this methodology since this approach relies on the relative motion between interconnected lumped-masses.

Similar to the previous scenario, in state#03 the structure underwent a change in the mass (i.e., 19.1% mass increment), but in this case, the additional mass was placed at the first-floor plate. The values obtained for $\Delta\mu/\mu_r$ showed a reduction of 18.1% in the mean of the identified mass-normalized stiffness-like coefficient for the first-floor element $G^{(1)}$, while relatively low changes, around 1%, were observed in the second and third-storey elements $G^{(2)}$ and $G^{(3)}$. In addition, the mean values of the mass-normalized damping-like terms also changed by 15.2%, 9.4% and 25.9% in the first, second and third floor, respectively. By examining the values of $\Delta\mu/\sigma_r$, it is clear that only the $a_{10}^{(1)}$ term with the largest signal-to-noise ratio ($\Delta\mu/\sigma_r = -4.480$) for this scenario had a significant reduction in the coefficient's mean with respect to the reference case; while the variations in the other coefficients were negligible. Keeping in mind that changes in $a_{10}^{(i)}$ coefficients can be caused by modifications in either or both the mass and stiffness; hence, additional assumptions and/or tests have to be made in order to infer further information about how those physical parameters have been modified. This can be achieved by experimentally estimating the mass in the sections of the chain-like system where the structural change have been located. Detailed description of several approaches for mass estimation can be found in [27,37–39]. Assuming that only changes in mass could occur in this scenario, the observed reduction in the $a_{10}^{(1)}$ coefficient would correspond to a 22.1% increment in the first-floor mass, which is fairly close to the actual 19.1% additional mass.

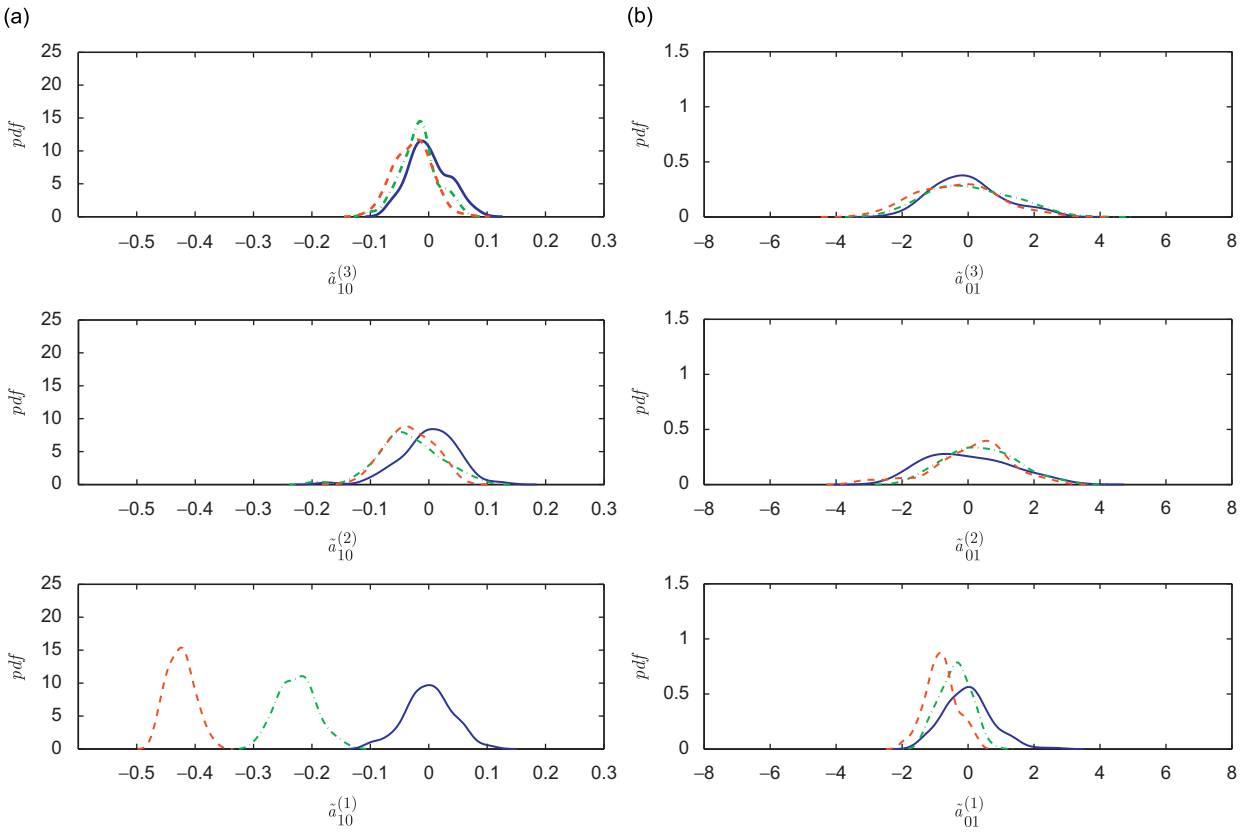

Fig. 6. Comparison of probability density functions of identified mass-normalized stiffness-like and mass-normalized damping-like coefficients. The solid lines correspond to the pdf of the coefficients in the baseline condition. The dot-dashed and dashed lines show the coefficients' pdf obtained in state#4 and state#5, respectively. (a) Normalized stiffness-like coefficients ($\tilde{a}_{10}^{(i)}$) and (b) Normalized damping-like coefficients ($\tilde{a}_{01}^{(i)}$).

In Fig. 5(a), the estimated probability density functions of the reference-normalized $\tilde{a}_{10}^{(i)}$ coefficients obtained for state#2 (dot-dashed lines) and state#3 (dashed lines) are compared with the baseline distributions from state#1 (solid lines). Clearly, the only significant shift in the mass-normalized stiffness-like coefficients is observed in the structure's first-floor. In the second and third floor no difference in the coefficients' distributions were observed after introducing the structural change. From inspection of Fig. 5(b), it is easily seen that the probability distributions of the mass-normalized damping-like coefficients did not differ appreciably among the different structural conditions.

In state#4 the stiffness of the first floor was decreased by 21.88% by introducing a 87.5% stiffness reduction in one of the four columns of the corresponding storey. Similarly, a 43.75% floor stiffness reduction was obtained for state#5 by decreasing the stiffness of two columns by a 87.5%. Since the structural changes in these scenarios consisted of column-stiffness reductions, it was expected that the estimated first-floor stiffness-like coefficients would have the largest and most significant variations among all other coefficients. By comparing the indices $\Delta\mu/\sigma_r$ listed in Table 3, it is worth noting that the detected relative changes in the mean of the identified coefficient $a_{10}^{(1)}$, for each of the above mentioned scenarios, had in overall the highest levels of significance, with corresponding values of $\Delta\mu/\sigma_r = -5.579$ and $\Delta\mu/\sigma_r = -10.506$. As previously discussed, these results mean that significant and observable differences exist between the $a_{10}^{(1)}$ coefficients from the baseline condition and each of the cases under discussion. Besides, the results also showed that *no* false-positive changes in coefficients $a_{10}^{(2)}$ and $a_{10}^{(3)}$ were detected. To appreciate the capability of the presented methodology to assess the level of change in the structure, a simple inspection of the $\Delta\mu/\mu_r$ indices for the relevant coefficient is needed. The values of the corresponding detected mean changes in the first-floor stiffness-like coefficient were $\Delta\mu/\mu_r = -0.226$ and $\Delta\mu/\mu_r = -0.425$ for the state#4 and state#5, respectively. The magnitude of the identified mean reductions in $a_{10}^{(1)}$ correlate quite well with the real storey-stiffness reductions in the experimental model. Notice that detected changes were proportional to the magnitude of the structural modification introduced in the system. Analysis of the probability density functions depicted in Fig. 6 will lead to conclusions similar to the already described findings.

For the scenarios of state#6 through state#9, the normalized indices (Table 3) and the density distributions of the $a_{10}^{(i)}$ coefficients (Figs. 7–8), also showed the presence of statistically significant changes in the mass-normalized stiffness-like coefficients of the second and third floors. The magnitude and location of the detected changes closely agree with the

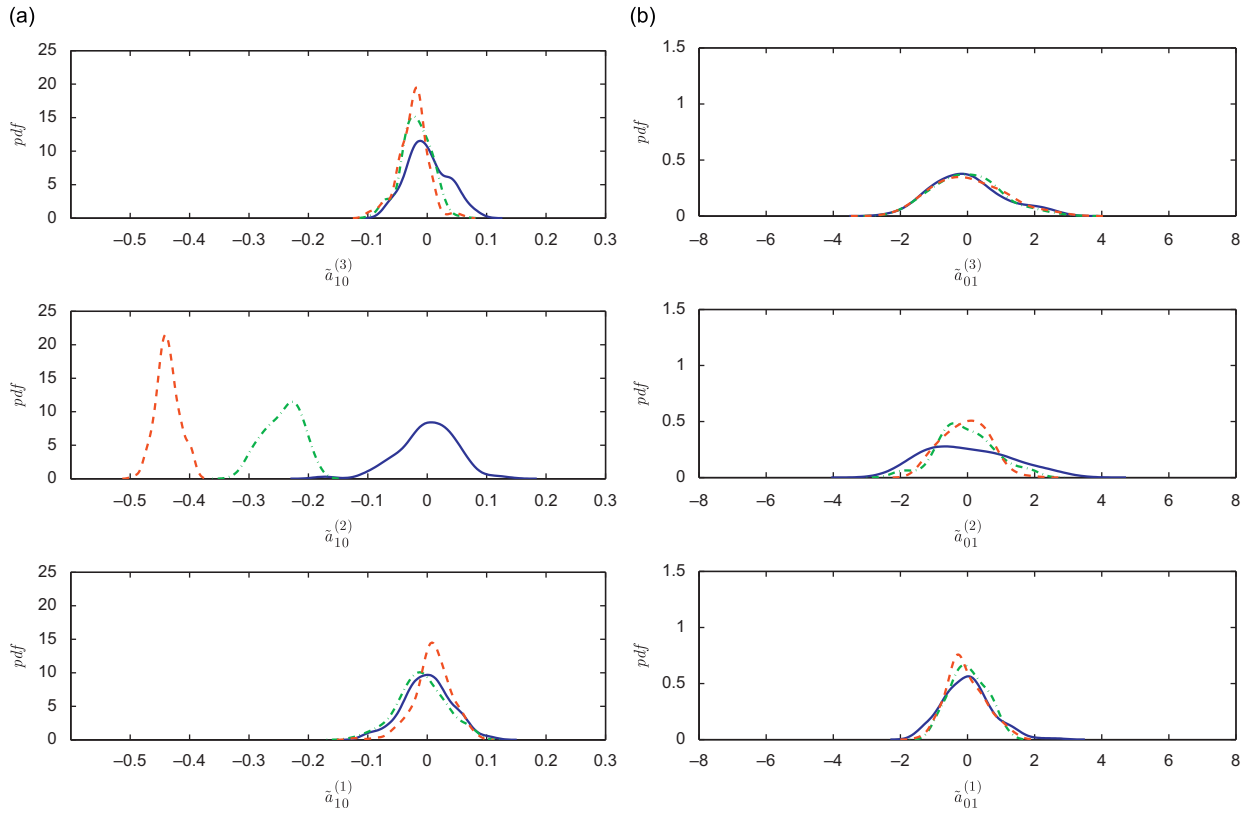

Fig. 7. Comparison of probability density functions of identified mass-normalized stiffness-like and mass-normalized damping-like coefficients. The solid lines correspond to the pdf of the coefficients in the baseline condition. The dot-dashed and dashed lines show the coefficients' pdf obtained in state#6 and state#7, respectively. (a) Normalized stiffness-like coefficients ($\tilde{a}_{10}^{(i)}$) and (b) Normalized damping-like coefficients ($\tilde{a}_{01}^{(i)}$).

actual stiffness modifications introduced in system. Also note that no false-positives in the $a_{10}^{(i)}$ coefficients were observed for these scenarios. In contrast, the mass-normalized damping-like coefficients did not provide any useful information about the condition of the structural system.

The results of this experimental study showed that the proposed detection approach for chain-like systems was able, in a rigorous statistical framework and despite the inherent randomness in the dominant restoring force coefficients, to confidently detect the presence of structural changes, accurately locate the structural section where the change occurred (i.e., first-floor, second-floor or third-floor), and provide an accurate estimate of the actual level of "change". It is important to point out that, for the established decision rule $|\Delta\mu/\sigma_r| \geq 2.0$, the minimum detectable (relative) change (*MDC*) in the identified restoring force coefficients that can be reliably detected is given by $MDC = 2.0\delta_r$, where δ_r indicates the coefficient of variation of the coefficients from the reference condition. For the mass-normalized stiffness-like terms $a_{10}^{(i)}$, the corresponding minimum detectable changes were 8%, 9% and 7% for the first, second and third floor, respectively. Since the magnitude of the structural changes was estimated quite accurately, it can be assumed that, relative structural changes in the floor stiffness and mass of the LANL test-bed structure below an approximate 9% could *not* be *reliable* detected by this proposed SHM methodology.

3.5. Global modal analysis

A full-order finite element model of the test structure, as well as the results from the experimental modal identification using the ERA algorithm [40] were employed to validate the effectiveness of proposed change detection approach based on the chain system identification methodology. The identification of the mass-normalized stiffnesses from the experimental modal parameters (i.e., eigenvalues and mode shapes) was carried out through the least-squares solution of the associated eigenvalue problem [41]. Similar to the chain-like system identification, the variations in the mass-normalized stiffnesses can be caused by either changes in the mass or the stiffness of the structure. Therefore, a mass estimation would be necessary in order to differentiate the type of structural change. Tables 4 and 5 summarize the relative changes ($\Delta\mu/\mu_r$) and signal-to-noise ratios ($\Delta\mu/\sigma_r$) of the mass-normalized stiffnesses $\overline{k}_i$ estimated from the analytical model (FEM),

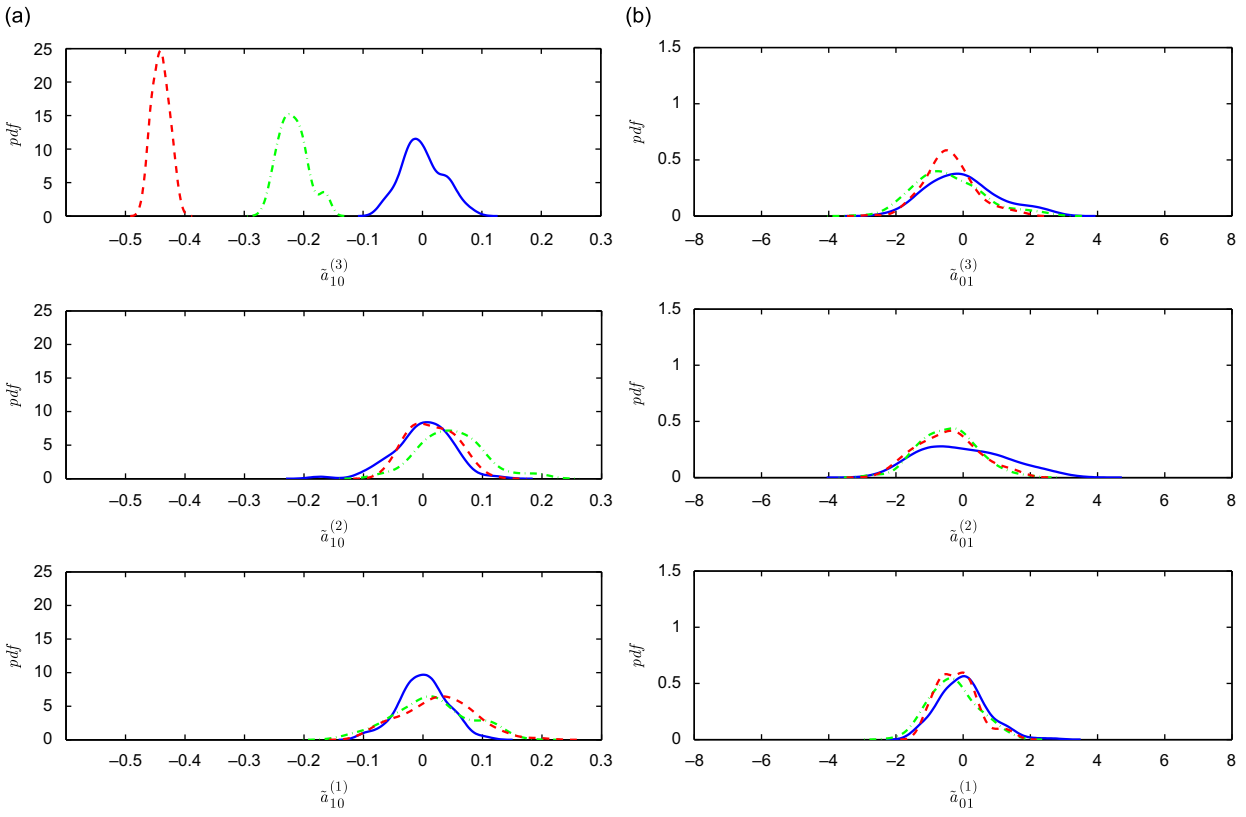

Fig. 8. Comparison of probability density functions of identified mass-normalized stiffness-like and mass-normalized damping-like coefficients. The solid lines correspond to the pdf of the coefficients in the baseline condition. The dot-dashed and dashed lines show the coefficients' pdf obtained in state#8 and state#9, respectively. (a) Normalized stiffness-like coefficients ($\tilde{a}_{10}^{(i)}$) and (b) Normalized damping-like coefficients ($\tilde{a}_{01}^{(i)}$).

Table 3
Summary of relative mean change ($\Delta\mu/\mu_r$) and signal-to-noise ratio ($\Delta\mu/\sigma_r$) in the identified restoring force coefficients for the LANL test-bed structure.

State	1st floor				2nd floor				3rd floor			
	$a_{10}^{(1)}=\overline{k}_1$		$a_{01}^{(1)}=\overline{c}_1$		$a_{10}^{(2)}=\overline{k}_2$		$a_{01}^{(2)}=\overline{c}_2$		$a_{10}^{(3)}=\overline{k}_3$		$a_{01}^{(3)}=\overline{c}_3$	
	$\Delta\mu/\mu_r$	$\Delta\mu/\sigma_r$	$\Delta\mu/\mu_r$	$\Delta\mu/\sigma_r$	$\Delta\mu/\mu_r$	$\Delta\mu/\sigma_r$	$\Delta\mu/\mu_r$	$\Delta\mu/\sigma_r$	$\Delta\mu/\mu_r$	$\Delta\mu/\sigma_r$	$\Delta\mu/\mu_r$	$\Delta\mu/\sigma_r$
State#2	−0.012	−0.285	−0.019	−0.027	0.005	0.100	−0.393	−0.320	−0.001	−0.023	0.036	0.034
State#3	**−0.181**	**−4.480**	−0.152	−0.213	−0.009	−0.179	0.094	0.076	−0.005	−0.130	0.259	0.245
State#4	**−0.226**	**−5.579**	−0.394	−0.549	−0.034	−0.695	0.389	0.317	−0.017	−0.491	0.074	0.070
State#5	**−0.425**	**−10.506**	−0.815	−1.138	−0.033	−0.678	0.118	0.096	−0.028	−0.796	−0.346	−0.328
State#6	−0.010	−0.235	0.027	0.038	**−0.243**	**−5.019**	−0.040	−0.033	−0.018	−0.523	−0.001	−0.001
State#7	0.009	0.229	−0.046	−0.064	**−0.437**	**−9.019**	−0.067	−0.055	−0.024	−0.689	0.039	0.037
State#8	0.014	0.352	−0.281	−0.393	0.049	1.002	−0.449	−0.365	**−0.217**	**−6.257**	−0.421	−0.398
State#9	0.025	0.629	−0.175	−0.244	0.015	0.312	−0.468	−0.381	**−0.441**	**−12.688**	−0.401	−0.379

Boldfaced table entries correspond to the detected structural changes.

experimental modal analysis (ERA), and the proposed algorithm (ChainID). Table entries in boldface correspond to actual structural changes that were detected correctly while the underlined ones were false positives.

From simple inspection of the tabulated $\Delta\mu/\mu_r$ values (Table 4), it can be observed that both the ERA and ChainID algorithms were capable of estimating, with very good level of accuracy, the magnitude of the different structural changes to which the LANL test-bed system was subjected to. However, by comparing the $\Delta\mu/\sigma_r$ indices in Table 5, the chain-like system identification methodology is shown to have better detection robustness than the eigensystem realization algorithm. No false-positive changes were detected by the approach proposed in this paper while the ERA had a false-positive rate of 35.3% (6/17). Notice that this rate depends on the threshold for $\Delta\mu/\sigma_r$, and it clearly can be increased or reduced by varying the levels of confidence. Keep in mind that the condition $|\Delta\mu/\sigma_r| \geq 2.0$ was assumed in order to

Table 4
Global system identification.

State	$\Delta\mu/\mu_r$								
	$\overline{k}_1$			$\overline{k}_2$			$\overline{k}_3$		
	FEM	ERA	ChainID	FEM	ERA	ChainID	FEM	ERA	ChainID
State#2	–	−0.098	−0.012	–	0.029	0.005	–	−0.005	−0.001
State#3	**−0.160**	**−0.102**	**−0.181**	–	−0.110	−0.009	–	0.037	−0.005
State#4	**−0.218**	**−0.196**	**−0.226**	–	−0.006	−0.034	–	0.003	−0.017
State#5	**−0.437**	**−0.390**	**−0.425**	–	−0.026	−0.033	–	0.008	−0.028
State#6	–	−0.009	−0.01	**−0.218**	**−0.240**	**−0.243**	–	−0.036	−0.018
State#7	–	−0.032	0.009	**−0.437**	**−0.456**	**−0.437**	–	−0.059	−0.024
State#8	–	−0.007	0.014	–	−0.008	0.049	**−0.218**	**−0.213**	**−0.217**
State#9	–	0.001	0.025	–	−0.021	0.015	**−0.437**	**−0.425**	**−0.441**

Comparison of $\Delta\mu/\mu_r$ in the identified mass-normalized stiffnesses for LANL test-bed structure. Boldfaced table entries correspond to the actual structural changes and false positives, respectively.

Table 5
Global system identification.

State	$\Delta\mu/\sigma_r$					
	$\overline{k}_1$		$\overline{k}_2$		$\overline{k}_3$	
	ERA	ChainID	ERA	ChainID	ERA	ChainID
State#2	−3.260	−0.285	2.013	0.100	−0.496	−0.023
State#3	**−3.388**	**−4.480**	−7.610	−0.179	3.447	−0.130
State#4	**−6.514**	**−5.579**	−0.414	−0.695	0.293	−0.491
State#5	**−12.968**	**−10.506**	−1.815	−0.678	0.821	−0.796
State#6	−0.300	−0.235	**−8.575**	**−5.019**	−3.415	−0.523
State#7	−1.066	0.229	**−17.029**	**−9.019**	−5.542	−0.689
State#8	−0.236	0.352	−0.552	1.002	**−9.807**	**−6.257**
State#9	0.037	0.629	−1.480	0.312	**−19.569**	**−12.688**

Comparison of $\Delta\mu/\sigma_r$ in the identified mass-normalized stiffnesses for LANL test-bed structure. Boldfaced and underlined table entries correspond to the actual structural changes and false positives, respectively.

Table 6
Comparison of numerical and experimental modal parameters.

Mode	f (Hz)			ζ (%)	
	FEM	ERA	ChainID	ERA	ChainID
1	29.90	30.81	31.38	4.17	4.37
2	55.46	55.38	59.19	1.49	1.90
3	72.60	71.11	75.39	0.64	0.94

detect structural changes beyond the 95% confidence intervals of the reference distributions. The minimum detectable change ($MDC = 2.0\delta_r$) in the mass-normalized stiffnesses identified with ERA was found to be around 6%. However, because of the high rate of false-positives obtained with ERA, it is not possible to assume that the estimated *MDC* would be a good indication for the minimum structural change that can be detected by this approach.

Even though the use of modal properties to detect changes in the structure were out of the scope of this study, it was interesting to check the consistency in the parameters obtained by a global identification techniques such as ERA, and the presented methodology. The numerical and experimental frequencies, as well as the damping ratios, for the reference condition are shown in Table 6. For all other scenarios, only the relative changes in natural frequencies were summarized in Table 7. It can be seen that frequency changes, for some specific scenarios and modes, were better estimated by either the ERA or the ChainID method, but generally speaking, both approaches exhibited similar performance. Furthermore, these results show some of the limitations that modal-based detection techniques, especially those using natural frequencies, can experience in detecting, locating and estimating the level of damage in real structures.

Table 7
Relative changes in experimentally identified natural frequencies.

State	$\Delta\mu/\mu_r$								
	f_1			f_2			f_3		
	FEM	ERA	ChainID	FEM	ERA	ChainID	FEM	ERA	ChainID
State#2	−0.036	−0.013	−0.000	−0.019	−0.021	−0.003	−0.005	−0.006	−0.007
State#3	−0.006	0.003	−0.027	−0.021	−0.016	−0.050	−0.031	−0.035	−0.026
State#4	−0.034	0.004	−0.043	−0.063	−0.063	−0.067	−0.023	−0.022	−0.039
State#5	−0.094	−0.021	−0.111	−0.133	−0.143	−0.156	−0.040	−0.041	−0.080
State#6	−0.065	−0.032	−0.079	0.001	0.006	−0.007	−0.052	−0.069	−0.061
State#7	−0.157	−0.081	−0.164	−0.013	0.014	−0.006	−0.108	−0.133	−0.102
State#8	−0.035	−0.021	−0.022	−0.062	−0.064	−0.059	−0.023	−0.022	−0.007
State#9	−0.095	−0.057	−0.094	−0.132	−0.135	−0.134	−0.039	−0.039	−0.027

4. Summary and conclusions

An experimental study is performed to evaluate the effectiveness and reliability of a SHM methodology for uncertain MDOF chain-like systems, built on a data-driven non-parametric identification technique. The relatively simple computational procedures and the decomposition scheme makes this approach suitable for being adopted in small wireless embedded sensor nodes. Even though this SHM approach can only be implemented for a specific type of structures, the chain-like system topology encompasses many practical applications in the aerospace, civil and mechanical engineering fields (e.g., tall buildings, transmission towers, offshore platforms, wind turbines and airplane wings).

The data-driven non-parametric identification approach, based on the *Restoring Force Method*, is used to develop a reduced-order model-free representation for each of the interconnecting elements in the MDOF chain-like system, by determining the dominant power-series coefficients (i.e., restoring force coefficients) that characterize the governing dynamic features of the system. This makes the restoring force coefficients a suitable set of parameters for change detection applications. Experimental data (only the acceleration time-histories) from a test-bed structure, that has been tested at the Los Alamos National Laboratory (LANL), were used to illustrate the implementation of this approach.

The experimental results clearly demonstrate the effectiveness and robustness of the proposed SHM scheme and the chain-like system identification method to confidently *detect* and *locate* structural changes in the system despite the modeling, measurement and data processing uncertainties. Moreover, it is shown that the dominant restoring force coefficients, which proved to be reliable change-sensitive features, can be used in a rigorous statistical framework not only for detecting and assessing the magnitude of the changes, and quantifying the detection uncertainty, but also for estimating the level of minimum detectable changes in the restoring force coefficients that can be reliably identified by this proposed SHM methodology.

A full-order finite element model of the test structure, as well as the results from the experimental modal identification using the ERA algorithm were employed to validate the results obtained by the proposed identification approach. Although both experimental algorithms were capable of estimating, with very good level of accuracy, the magnitude of the actual structural changes, the chain-like system identification methodology clearly showed that it is more reliable and has better detection rate than the ERA method.

It is important to note that, the methodology presented in this study was demonstrated by detecting changes in the mass and stiffness of a small-scale structure tested in a well-controlled laboratory setting and as such, the influence of nonlinearities and the effect of operational and environmental conditions were not incorporated into this study. Furthermore, the actual physical changes made in the structure were quite severe and not representative of realistic scenarios likely to be encountered in practical field implementations. None the less, as long as the effects of operational and environmental conditions, and underlying damage mechanisms in a target structure are reflected in the monitored structural dynamic response, then the method under discussion may provide a useful tool to accurately detect, locate (within each "decomposed" structural region), and quantify the level of damage as reflected in the identified restoring force surface.

Acknowledgment

This study was supported in part by a grant from the National Science Foundation.

References

[1] A. Guemes (Ed.), Structural Health Monitoring, *Proceedings of the Third European Workshop*, DEStech Publications, Inc, 2006.
[2] F.-K. Chang (Ed.), Structural Health Monitoring: Quantification, Validation and Implementation, DEStech Publications Inc, 2007.
[3] F. Casciati (Ed.), *Proceedings of the Third World Conference on Structural Control*, Wiley, New York, 2002.

[4] E.A. Johnson, A.W. Smith (Eds.), *Proceedings of the Fourth World Conference on Structural Control and Monitoring*, 2006.
[5] M. Tomizuka (Ed.), *Proceeding of SPIE Sensors and Smart Structures Technologies for Civil*, Mechanical, and Aerospace Systems, SPIE, 2008.
[6] M. Ahmadian (Ed.), *Proceeding of SPIE Active and Passive Smart Structures and Integrated Systems*, SPIE, 2008.
[7] D.E. Adams, *Health Monitoring of Structural Materials and Components: Methods with Applications*, Wiley, Chichester, England, 2007.
[8] G. Hackmann, F. Sun, N. Castaneda, C. Lu, S. Dyke, A holistic approach to decentralized structural damage localization using wireless sensor networks, *Proceedings of 29th IEEE Real-Time Systems Symposium*, 2008.
[9] T. Nagayama, B.F. Spencer, Structural Health Monitoring Using Smart Sensors, Technical Report NSEL-001, Newmark Structural Engineering Laboratory, University of Illinois at Urbana-Champaign, 2007.
[10] Y. Gao, B.F. Spencer, M. Ruiz-Sandoval, Distributed computing strategy for structural health monitoring, *Structural Control and Health Monitoring* 13 (2006) 488–507.
[11] S.W. Doebling, C.R. Farrar, M.B. Prime, D.W. Shevitz, Damage Identification and Health Monitoring of Structural and Mechanical Systems from Changes in their Vibration Characteristics: A Literature Review, Technical Report LA-13070, Los Alamos National Laboratory, 2007.
[12] B. Peeters, G. De Roeck, Stochastic system identification for operational modal analysis: a review, *ASME Journal of Dynamic Systems, Measurement, and Control* 123 (4) (2001) 659–667.
[13] H. Sohn, C.R. Farrar, F.M. Hemez, D.D. Shunk, D.W. Stinemates, B.R. Nadler, A Review of Structural Health Monitoring Literature: 1996–2001, Technical Report, LA-13976, Los Alamos National Laboratory, 2003.
[14] H. Van der Auweraer, B. Peeters, International research projects on structural health monitoring: an overview, *Structural Health Monitoring* 2 (2003) 341–358.
[15] W. Staszewski, C. Boler, G.R. Tomlinson, *Health Monitoring of Aerospace Structures: Smart Sensing Technologies and Signal Processing*, Wiley, Chichester, England, 2004.
[16] D.J. Inman, C.R. Farrar, V. Lopes, V. Steffen, *Damage Prognosis: For Aerospace, Civil and Mechanical Systems*, Wiley, Chichester, England, 2005.
[17] G. Kerschen, K. Worden, A.F. Vakakis, J.C. Golinval, Past, present and future of nonlinear system identification in structural dynamics, *Mechanical Systems and Signal Processing* 20 (2006) 505–592.
[18] H. Park, H. Sohn, Parameter estimation of the generalized extreme value distribution for structural health monitoring, *Probabilistic Engineering Mechanics* 21 (4) (2006) 366–376.
[19] J. Brownjohn, Structural health monitoring for civil infrastructure, *Philosophical Transactions of The Royal Society A* 365 (2007) 589–622.
[20] C.R. Farrar, K. Worden, M.D. Todd, G. Park, J. Nichols, D.E. Adams, M.T. Bement, K. Farinholt, Nonlinear System Identification for Damage Detection, Technical Report, LA-14353, Los Alamos National Laboratory, 2007.
[21] C.R. Farrar, K. Worden, An introduction to structural health monitoring, *Philosophical Transactions of The Royal Society A* 365 (2007) 303–315.
[22] M. Friswell, Damage identification using inverse methods, *Philosophical Transactions of The Royal Society A* 365 (2007) 393–410.
[23] S. Glaser, H. Li, M. Wang, J. Ou, J. Lynch, Sensor technology innovation for advancement of structural health monitoring: a strategic program plan of US-China research for the next decade, *Smart Structures & Systems* 3 (2) (2007) 221–244.
[24] J. Lynch, An overview of wireless structural health monitoring for civil structures, *Philosophical Transactions of The Royal Society A* (2007) 345–372.
[25] G. Park, D.J. Inman, Structural health monitoring using piezoelectric impedance measurements, *Philosophical Transactions of The Royal Society A* 365 (2007) 373–392.
[26] H. Sohn, Effects of environmental and operational variability on structural health monitoring, *Philosophical Transactions of The Royal Society A* 365 (2007) 539–560.
[27] S.F. Masri, G.A. Bekey, H. Sassi, T.K. Caughey, Non-parametric identification of a class of non-linear multidegree dynamic systems, *Earthquake Engineering and Structural Dynamics* 10 (1982) 1–30.
[28] S.F. Masri, J.P. Caffrey, T.K. Caughey, A.W. Smith, A.G. Chassiakos, A general data-based approach for developing reduced-order models of nonlinear MDOF systems, *Nonlinear Dynamics* 39 (2005) 95–112.
[29] S.F. Masri, R. Ghanem, F. Arrate, J.P. Caffrey, Stochastic nonparametric models of uncertain hysteretic oscillators, *AIAA Journal* 44 (10) (2006) 2319–2330.
[30] S.F. Masri, R. Ghanem, R. Govindan, R. Nayeri, A decentralized procedure for structural health monitoring of uncertain nonlinear systems provided with dense active sensor arrays, *Smart Materials and Structures* 17(4) (2008).
[31] K. Worden, G.R. Tomlinson, *Nonlinearity in Structural Dynamics: Detection, Identification and Modelling*, Institute of Physics, London, 2001.
[32] R.D. Nayeri, S.F. Masri, R.G. Ghanem, R.L. Nigbor, A novel approach for the structural identification and monitoring of a full-scale 17-storey building based on ambient vibration measurements, *Smart Materials and Structures* 17(2) (2008).
[33] S.F. Masri, T.K. Caughey, A nonparametric identification technique for nonlinear dynamic problems, *Journal of Applied Mechanics* 46 (1979) 433–447.
[34] H.-B. Yun, S.F. Masri, Stochastic change detection in uncertain nonlinear systems using reduced-order models: system identification, *Smart Materials and Structures* 17(1) (2008).
[35] E. Figueiredo, G. Park, J. Figueiras, C.R. Farrar, K. Worden, Structural Health Monitoring Algorithm Comparisons Using Standard Data Sets, Technical Report LA-14393, Los Alamos National Laboratory, 2009.
[36] R. Ghanem, S.F. Masri, M. Pellissetti, R. Wolfe, Identification and prediction of stochastic dynamical systems in a polynomial chaos basis, *Computer Methods in Applied Mechanics and Engineering* 194 (12–16) (2005) 1641–1654.
[37] K.J. O'Donnell, E.F. Crawley, Identification of Nonlinear System Parameters in Space Structure Joints Using the Force-State Mapping Technique, Technical Report, Report 16–85, MIT SSL, 1985.
[38] K. Worden, G.R. Tomlinson, Application of the restoring force surface method to nonlinear elements, *Proceedings of the Seventh IMAC*, Vol. II, 1989, pp. 1347–1355.
[39] M.A. Al-Hadid, J.R. Wright, Estimation of mass and modal mass in the identification of non-linear single and multi degree of freedom systems using the force-state mapping approach, *Mechanical Systems and Signal Processing* 6 (4) (1992) 383–401.
[40] J.N. Juang, R.S. Pappa, An eigensystem realization algorithm for modal parameter identification and model reduction, *AIAA Journal of Guidance, Control, and Dynamics* 8 (5) (1985) 620–627.
[41] J.M. Caicedo, S.J. Dyke, E.A. Johnson, NExT and ERA for phase I of the IASCE-ASCE benchmark problem: simulated data, *ASCE Journal of Engineering Mechanics* 130 (1) (2004) 49–60.